

Isolated Chargers for EVs Incorporating Six-Phase Machines

Ivan Subotic, *Student Member, IEEE*, Nandor Bodo, Emil Levi, *Fellow, IEEE*, Martin Jones, Victor Levi, *Senior Member, IEEE*

Abstract—The paper considers two isolated solutions for fast charging of electric vehicles (EVs). The isolation is located on the grid side (off-board), while the rest of the charging apparatus is placed on-board the EV and it entirely consists of the existing power electronics components that would be otherwise used only for propulsion. Thus, substantial savings on the space, weight, and cost are achieved. The considered configurations fully incorporate either a symmetrical or an asymmetrical six-phase machine, as well as a six-phase inverter, into the charging process. Due to the nature of the connections, torque production is avoided during the charging/vehicle-to-grid (V2G) modes of operation. Thus the machines do not have to be mechanically locked, and their rotors naturally stay at standstill. Control schemes for both configurations are elaborated, and theoretical results are validated by experiments for the two configurations in both charging and V2G modes.

Index Terms—Battery chargers, electric vehicles, integrated on-board chargers, six-phase machines.

I. INTRODUCTION

One of the main challenges in electric vehicle (EV) sector is to decrease the charging time of on-board battery chargers. Although this can be easily achieved by placing a high power standalone charger on-board the vehicle, this solution is not viable due to the unacceptable increase of vehicle weight and cost. A possible solution to overcome this problem is the use of integrated chargers. The idea is to reuse the existing components of an EV, predominantly the inverter and the propulsion machine, during the battery charging. This reduces the number of required new elements, thus naturally reducing the cost, weight and the required space.

Although non-isolated charging that complies with all safety regulations is possible, a preferable feature of battery chargers is galvanic isolation from the grid. However, the majority of the integrated configurations proposed so far are non-isolated [1]. In order to achieve galvanic isolation without

a high cost, a configuration that uses a machine as a transformer during the charging process was proposed in [2]. However, rotating field is produced in the machine during the charging process, leading to non-zero torque production.

The impact of avoiding isolation for one of the currently most attractive fast charging configurations [3] is assessed in a study performed in [4]. It is shown that, if isolation does not exist, the common mode voltage appears between the battery and the ground. Since typically some small parasitic capacitances exist between the chassis of EV and its battery, this can cause problems in battery management system, as well as high displacement currents that can flow through the protection earth conductor. These currents can significantly exceed the permitted limit that is set due to safety concerns if a proper mitigating technique is not employed (one of these may be the integration of a filter capacitor between the protection earth conductor and the neutral conductor [4]).

Another important aspect of integrated battery chargers is whether or not a torque gets produced during the charging process. If it is produced the machine's rotor has to be mechanically locked, which causes low charging efficiency and increased noise and wear. It is relatively easy to avoid torque production in the machine if the charging is from a single-phase grid, and this is why the majority of existing integrated charging solutions are viable only for single-phase charging [5-11]. However, the power is limited, so that only slow charging is possible with these configurations.

With regard to the charging from three-phase mains (fast charging), there are only a few configurations [3, 12-16] that are capable of integrating an induction or PM machine into the charging process without a torque production. A quantitative comparison of the solutions is given in Table I. This paper analyses the only two isolated configurations listed in Table I. These were originally introduced at the theoretical/simulation level in [15, 16]. Both avoid the additional isolation weight by displacing the isolation outside the vehicle into the charging station. In [15] a symmetrical six-phase machine is incorporated into the charging process, while [16] considers an asymmetrical six-phase configuration. The nature of the connections is such that the torque is not produced in the machine during the charging process in either of the two topologies.

The paper is organised as follows. In Section II operating principles are explained and theoretically assessed. A different grid connection topology, when compared to the solution in [15], for the symmetrical configuration is also detailed. Enhanced control for both configurations is described in Section III. Finally, theoretical results of Section II and the control principles of Section III are validated by experiments for both configurations, for both charging and V2G mode.

Manuscript received July 17, 2014; revised October 27, 2014 and January 12, 2015; accepted February 22, 2015.

Copyright © 2015 IEEE. Personal use of this material is permitted. However, permission to use this material for any other purposes must be obtained from the IEEE by sending the request to pubs-permissions@ieee.org.

The authors would like to acknowledge the Engineering and Physical Sciences Research Council (EPSRC) for supporting the Vehicle Electrical Systems Integration (VESI) project (EP/I038543/1).

I. Subotic, N. Bodo, E. Levi and M. Jones are with the School of Engineering, Technology and Maritime Operations, Liverpool John Moores University, Liverpool L3 3AF, UK (e-mail: i.subotic@2011.ljmu.ac.uk, n.bodo@2009.ljmu.ac.uk, e.levi@ljmu.ac.uk, m.jones2@ljmu.ac.uk).

V. Levi is with the School of Electrical and Electronic Engineering, The University of Manchester, Manchester M13 9PL, UK (e-mail: victor.levi@manchester.ac.uk).

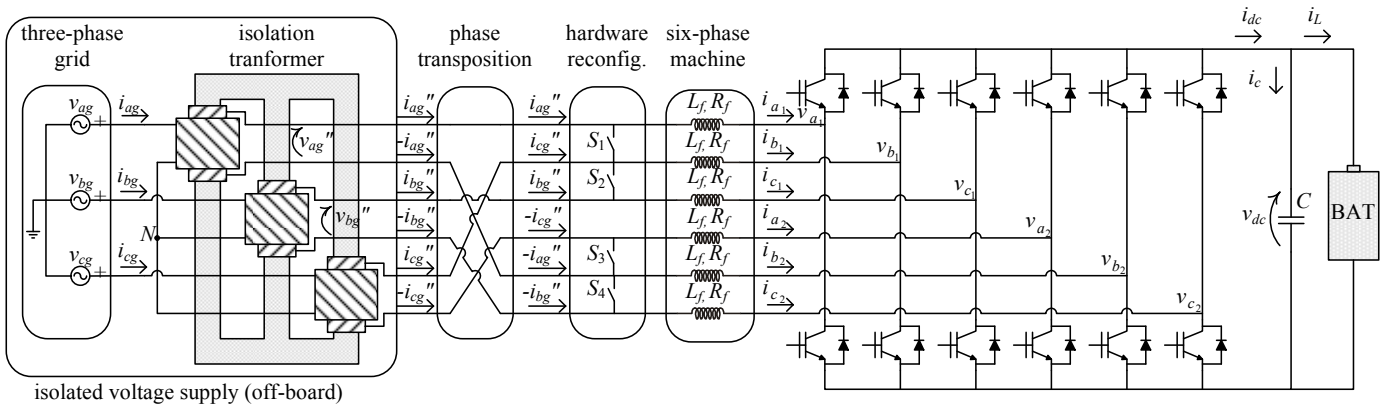


Fig. 1. Topology of the isolated charger incorporating a symmetrical six-phase machine. Grid connection system does not require a transformer with dual secondary (as in [15]) to create a symmetrical six-phase voltage supply for charging/V2G modes.

TABLE I
QUANTITATIVE COMPARISON OF THREE-PHASE CHARGING SOLUTIONS WITH INTEGRATED INDUCTION OR PM MACHINE WITHOUT THE TORQUE PRODUCTION

Ref.	Galvanic isolation	Low dc-bus voltage	Fault tolerance in propulsion mode	Hardware reconfiguration not required
[3]	x	x	✓	✓
[12]	x	x	✓	✓
[13]	x	✓	x	✓
[14]	x	x	x	x
[15]	✓	✓	✓	x
[16]	✓	x	✓	x

II. OPERATING PRINCIPLES OF SIX-PHASE CHARGING SYSTEMS

The original discussion of an integrated on-board battery charger, created using a symmetrical six-phase machine, was based on utilisation of a transformer with dual secondary windings and 180° phase shift between the outputs of the two secondary sets [15]. An alternative configuration, which does not require a transformer with dual secondary windings and is studied here further on, is depicted in Fig. 1. The operating principles of the topology in [15] and the one in Fig. 1 are the same and the difference is in essence in the transformer supply (which is off-board).

During the propulsion mode the grid is not connected and switches S_1 - S_4 are closed. For the charging mode they have to be opened, which puts the symmetrical six-phase machine in an open-end winding configuration. The six machine's phase windings are then connected to six transformer secondary terminals, as shown in Fig. 1. The transformer secondary three-phase winding is utilised in an open-end winding (OeW) configuration, so that connection of two motor phases is possible to each of the transformer secondary phases. However, the connections to the machine are further realised according to the same connection principles as in [15], so that torque production in the machine is avoided.

It should be noted that a dc-dc converter may or may not exist between the battery and the voltage source converter in Fig. 1. Its existence or absence has no impact on the operating principles, this being a common feature with the topology of [12]. The dc-dc converter is not used in the experiments here and is therefore not dealt with further on. It suffices to say that, if there is a dc-dc converter, it has to enable bi-directional power flow.

The topology introduced in [16] utilizes an asymmetrical six-phase machine and it is presented in Fig. 2. The right-hand part of the configuration is the same as in Fig. 1. It can be seen that a transformer with dual secondary windings is used to provide isolation and the set of asymmetrical six-phase voltages. During the charging process the machine terminals are connected to the transformer secondary. However, the connections do not follow the natural order (i.e. phases a_1 , b_1 and c_1 of the machine to phases a_1 , b_1 and c_1 of the transformer, respectively). Instead, the principle of phase transposition [17] is used in order to avoid torque production in the machine, this being the same as in the case of Fig. 1. The transformer with dual secondary windings is used since a transformer with OeW secondary cannot provide voltages that would completely displace excitation from the first (torque producing) into the second plane. Both solutions require a six-phase cable, which would be of the same total active cross-section as a three-phase one for the given charging power.

In order to assess machine's behaviour in the two topologies, decoupling transformation matrices are considered next. This is done separately for the two configurations.

A. Symmetrical System

The decoupling transformation matrix for the symmetrical six-phase systems is available in [15, 18]. Its application yields 2D components in two orthogonal planes, which can be given using complex space vectors as:

$$\begin{aligned} \underline{f}_{\alpha\beta} &= \sqrt{2/6} (f_{a_1} + \underline{a}^2 f_{b_1} + \underline{a}^4 f_{c_1} + \underline{a}^1 f_{a_2} + \underline{a}^3 f_{b_2} + \underline{a}^5 f_{c_2}) \\ \underline{f}_{xy} &= \sqrt{2/6} (f_{a_1} + \underline{a}^4 f_{b_1} + \underline{a}^8 f_{c_1} + \underline{a}^2 f_{a_2} + \underline{a}^6 f_{b_2} + \underline{a}^{10} f_{c_2}) \end{aligned} \quad (1)$$

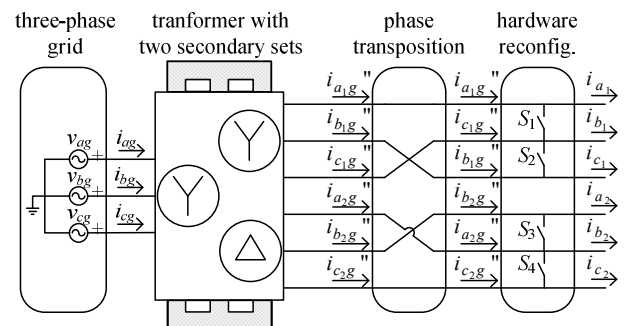


Fig. 2. Connections of isolated charger incorporating an asymmetrical six-phase machine (the right part is the same as in Fig. 1).

where $\underline{a} = \exp(j\delta) = \cos \delta + j \sin \delta$ and $\delta = 2\pi/6$ (which represents the spatial phase displacement between the two sets of three-phase windings). Symbol f stands for any variable that is being transformed (e.g. current, voltage, etc.), α - β are components in the torque-producing plane, and x - y are components in the second (non-torque producing) plane.

Grid currents at the secondary are governed with:

$$i_{kg}'' = \sqrt{2}I \cos(\omega t - l2\pi/3) \quad l=0,1,2 \quad k=a,b,c \quad (2)$$

From Fig. 1 it can be seen that the correlation of secondary currents and the currents that flow through the symmetrical six-phase machine is:

$$\begin{aligned} i_{a_1} &= i_{ag}'' & i_{b_1} &= i_{bg}'' & i_{c_1} &= i_{cg}'' \\ i_{a_2} &= -i_{cg}'' & i_{b_2} &= -i_{ag}'' & i_{c_2} &= -i_{bg}'' \end{aligned} \quad (3)$$

Substitution of (2) and (3) into (1) leads to the following two space vectors:

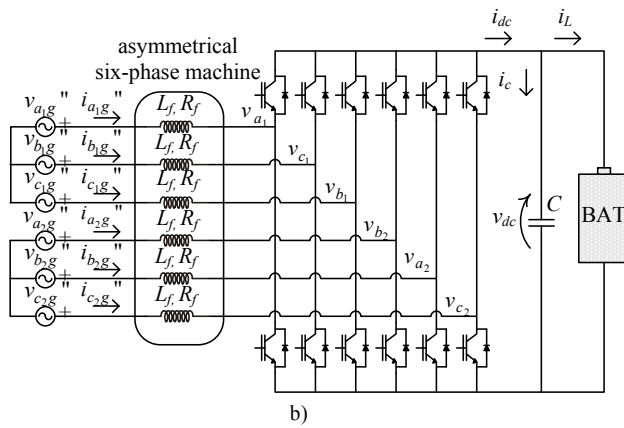
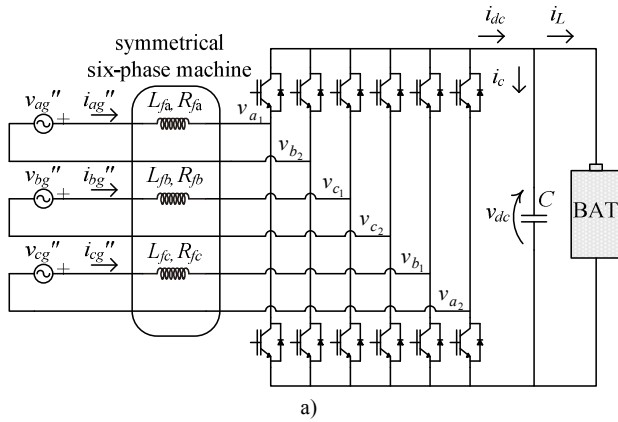


Fig. 3. Equivalent schemes for the configurations of a) Fig. 1, b) Fig. 2.

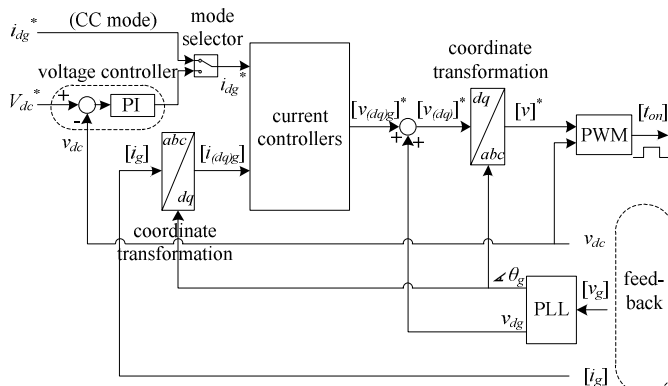


Fig. 4. Control algorithm for the charging/V2G mode for both configurations.

$$\underline{i}_{\alpha\beta} = \sqrt{6}I \cos(\alpha t) \quad (4)$$

$$\underline{i}_{xy} = j\sqrt{6}I \sin(\alpha t) \quad (5)$$

It can be seen that the first (torque-producing) plane has excitation. However, only the α -component is of non-zero value; thus the field in the machine rotor will be pulsating and hence not capable of producing a starting torque. Machine will, therefore, stay at standstill without any requirement for a mechanical brake.

B. Asymmetrical System

For the asymmetrical six-phase system the decoupling transformation matrix is different [18]. Expressing again the resulting 2D variables as complex quantities one now has:

$$\underline{f}_{\alpha\beta} = \sqrt{2/6} (f_{a_1} + \underline{a}^4 f_{b_1} + \underline{a}^8 f_{c_1} + \underline{a} f_{a_2} + \underline{a}^5 f_{b_2} + \underline{a}^9 f_{c_2}) \quad (6)$$

$$\underline{f}_{xy} = \sqrt{2/6} (f_{a_1} + \underline{a}^8 f_{b_1} + \underline{a}^{16} f_{c_1} + \underline{a}^5 f_{a_2} + \underline{a} f_{b_2} + \underline{a}^9 f_{c_2})$$

where $\underline{a} = \exp(j\delta) = \cos \delta + j \sin \delta$ and $\delta = \pi/6$ (spatial phase displacement between the two sets of windings). Grid currents at the output of the transformer are given with:

$$i_{k_1g} = \sqrt{2}I \cos(\omega t - l\pi/6) \quad l=0,4,8 \quad k=a,b,c \quad (7)$$

$$i_{k_2g} = \sqrt{2}I \cos(\omega t - l\pi/6) \quad l=1,5,9 \quad k=a,b,c$$

According to Fig. 2 their correlation with the machine's currents is:

$$i_{a_1} = i_{a_1g} \quad i_{b_1} = i_{c_1g} \quad i_{c_1} = i_{b_1g} \quad (8)$$

$$i_{a_2} = i_{b_2g} \quad i_{b_2} = i_{a_2g} \quad i_{c_2} = i_{c_2g}$$

Using (8) in conjunction with (6)-(7), the following two space vectors are obtained:

$$\underline{i}_{\alpha\beta} = 0 \quad (9)$$

$$\underline{i}_{xy} = \sqrt{6}I \exp(j\alpha t) \quad (10)$$

Clearly, the flux/torque producing plane (α - β) is not excited and the grid currents flow through the x - y plane, so that the machine stays at standstill. Zero-sequence components are both equal to zero.

III. CONTROL OF SIX-PHASE CHARGING SYSTEMS

Theoretical analysis in Section II implies that both symmetrical and asymmetrical six-phase machines, in configurations shown in Fig. 1 and Fig. 2, will act as passive resistive-inductive components during charging. Their equivalent models during the charging mode of operation are presented in Fig. 3a and Fig. 3b, respectively.

In the configuration of Fig. 2 only leakage flux appears in the machine during the charging process (9). Therefore, the equivalent scheme of the machine consists of stator leakage inductance and resistance (Fig. 3b). On the other hand, in the case of the topology of Fig. 1 a pulsating field gets produced in the rotor (4), so that mutual inductance and rotor parameters start to influence the system. As will be shown later, this influence varies among phases, and causes a difference between equivalent per-phase parameters of the machine. The correlation between the equivalent parameters for the charging mode and machine parameters is complex and is beyond the scope here. The fact that the equivalent parameters are not the same for all the phases is underlined in Fig. 3a by using different symbols.

In order to comply with grid requirements that only

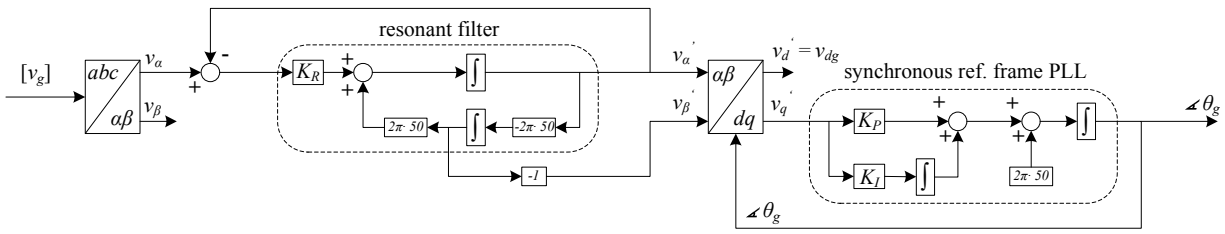


Fig. 5. Phase locked loop (PLL) algorithm.

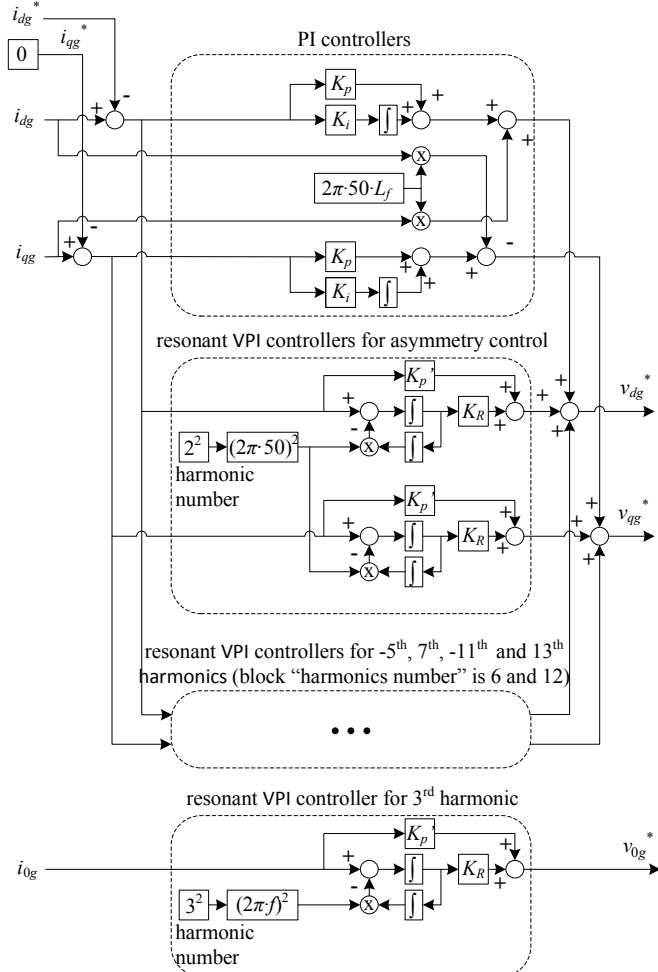


Fig. 6. Current controllers for the configuration of Fig. 3a.

sinusoidal currents, in phase with grid voltages, can be taken or injected into the grid, voltage oriented control is chosen for the control purposes. The control algorithm is the same for both cases and is given in Fig. 4. It should be noted that, in order to apply to both topologies, Fig. 4 utilizes suffix “dq” to represent all components that are obtained after rotational transformation. In the case of the symmetrical system these are dq0, while in the case of the asymmetrical system they are dqxy0₁0₂. Required feed-back signals are dc-bus voltage, grid phase voltages, and grid currents. However, grid current sensors are not required since grid currents can be obtained from machine current sensors, which are anyway compulsory for the propulsion mode.

The control for both configurations commences in the same manner, with calculation of the grid position from a phase-locked loop (PLL). The one shown in Fig. 5 is used, since it provides satisfactory performance even with distorted grid

voltages, as shown in [19]. The rest of the control scheme is considered separately for the two configurations.

A. Symmetrical Six-phase Configuration – Fig. 3a

The aim of the control is to place grid currents i_{ag} , i_{bg} , i_{cg} , in phase with grid phase voltages v_{ag} , v_{bg} and v_{cg} (to obtain unity power factor). This is accomplished by controlling the transformer secondary variables. In order to observe phase deviation of grid currents from grid phase voltages, the currents are transformed into grid voltage oriented reference frame. This is done by applying a decoupling transformation for the three-phase systems, and then the rotational transformation (in Fig. 4 these two are lumped together in one block called “coordinate transformation”). This is where information from the PLL, regarding the grid position, is utilized. Now, three current components are obtained; d -component is in phase with grid voltage space vector, q -component is shifted by ninety degrees, and zero-sequence component is the one that represents the sum of grid currents. In order to have unity power factor only the component in phase with the grid voltage, i.e. d -component, should have a nonzero value, while the reference for the other two components should be zero.

In constant current–constant voltage (CC–CV) charging strategy [20] there are two ways of obtaining the reference for the current d -component. In CV mode dc-bus voltage is regulated; thus the d -current reference is an output of a dc voltage controller (Fig. 4). In CC mode constant current is required, and therefore the reference is just the desired value of the grid current. In order to avoid dependence of battery charging power on grid voltage fluctuations this value can be obtained from an additional battery current PI controller.

When the current reference is obtained (in CC or CV mode) d -component of the grid current is controlled to follow it in the block “current controllers” in Fig. 4. Since it is a dc quantity it can be controlled with a simple PI controller shown at the top of Fig. 6. Similarly, the q -component is controlled to zero with a PI controller, and this suffices for the control of grid current fundamental in symmetrical (balanced) systems.

However, Fig. 3a demonstrates that equivalent machine parameters are not equal for the three phases (equivalent parameters have different symbols). This is caused by a pulsating field in the machine (which is predicted by (4)). When a field pulsates it induces some currents in the rotor; thus rotor resistance and leakage inductance start to influence the system (rotor losses produced in this way and associated thermal issues are beyond the scope of this paper). The rotor has the highest impact on phases that produce the most of the pulsating flux. The reason for this is that the rotor field is also pulsating. This flux is in the direction of the α -axis (4); thus phases that influence it the most are a_1 and b_2 , since they lay

on the α -axis. Therefore, the parameters L_{af} and R_{af} are the highest since they are influenced by resistance and leakage inductance of phases a_1 and b_2 in addition to the highest part of rotor resistance and leakage inductance.

The parameter asymmetry gets manifested through a fundamental component that rotates in anti-synchronous direction. From the d - q reference frame it is seen as the -2^{nd} harmonic (harmonic that has the frequency two times higher than synchronous and that rotates in the opposite direction). In order to have the same grid current amplitudes in three phases this component has to be controlled to zero. It can be controlled by a vector proportional-integral (VPI) resonant controller that is tuned to the second harmonic by the block “harmonic number” (middle part of Fig. 6).

On the other hand, grid current does not have only fundamental. Low-order odd harmonics are inevitably produced due to the inverter dead time, and they require control as well. In three-phase systems these are predominately the -5^{th} , 7^{th} , -11^{th} and 13^{th} harmonics (as seen from the stationary reference frame). The minus sign refers to the anti-synchronous direction of rotation. From the d - q (synchronous) reference frame these harmonics are seen as -6^{th} , 6^{th} , -12^{th} and 12^{th} harmonic, respectively. Since resonant controllers are capable of controlling the harmonics in both directions at the same time, single resonant controller tuned at the 6^{th} harmonic in one axis can control both the -6^{th} and 6^{th} harmonic (seen from the synchronous reference frame). Similarly, the one tuned at the 12^{th} harmonic can control both

-12^{th} and 12^{th} harmonic in one axis at the same time. Therefore, two VPI resonant controllers, placed in each axis, can control all four dominant harmonics (they are the same as a pair for asymmetry control in Fig. 6, and the only difference is in the block “harmonic number”, which in this case has values 6 and 12). VPI type of resonant controllers [21] is chosen since they are shown to be superior to standard PR controllers [22].

This is still not sufficient for the good current control of the configuration in Fig. 3a. As can be seen, the secondary side of the transformer does not have a neutral point (Fig. 3a). This means that zero-sequence current can flow on this side. Thus, unlike in standard three-phase systems, the harmonics that map into zero-sequence can flow. These are the harmonics whose order is a multiple of three, with the dominant 3^{rd} harmonic. This harmonic can be controlled using the zero-sequence current, with the VPI resonant controller tuned at the 3^{rd} harmonic frequency, as shown at the bottom of Fig. 6. It should be noted that, if transformer primary is grounded (as the case is in the performed experiments), zero-sequence harmonics can penetrate into the grid. It is also important to emphasise that the need for the zero-sequence current controller arises here due to the specific open-end secondary winding arrangement of Fig. 1. If a transformer with two three-phase secondaries, connected in star with isolated neutral points and with phase shifted outputs by 180° , is used instead (as in [15]) there is no need for the zero-sequence current control.

After transformation of the output of the current control block, the signals enter the carrier-based PWM unit, and this concludes the control algorithm. It should be noted that the zero-sequence injection cannot be utilized in the PWM to improve dc-bus voltage utilization, since it would cause zero-sequence currents at the transformer secondary.

B. Asymmetrical Six-phase Configuration – Fig. 3b

Control of the configuration shown in Fig. 3b is similar to the one described in the previous subsection, and the control scheme in Fig. 4 remains to be valid. However, there are three important differences. First of all, it can be seen from Fig. 3b that the equivalent phase parameters have the same symbols signifying their mutual equality; thus the system will be balanced, and there will be no need for asymmetry control. Next, zero-sequence harmonics cannot flow, which further simplifies the control. Finally, the third difference aggravates the control and is the consequence of the fact that there are now six different individual phase currents, which belong to two separate phase-shifted three-phase systems. The total number of the degrees of freedom is now four (zero-sequence currents cannot exist due to the star-delta connection of the secondaries), while it was three for the symmetrical configuration.

The control action again commences with the PLL and subsequent transformation of the transformer secondary set of currents into the rotational reference frame. However, the transformation is now for the six-phase rather than three-phase system. This means that it employs the asymmetrical six-phase decoupling transformation governed with (6), followed by the rotational transformation for the six-phase system. Hence the output contains six current components: d , q , x' , y' , $0+$ and $0-$.

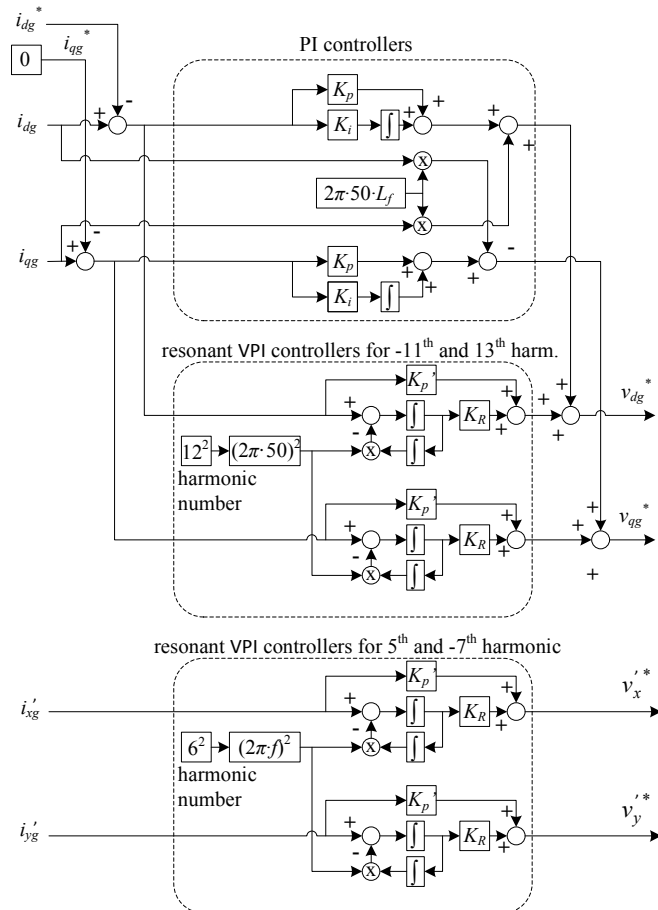


Fig. 7. Current controllers for the configuration of Fig. 3b.

Primed symbols used in conjunction with x - y components (i.e. x' and y') mean that they are transformed rotationally as well (into a reference frame that rotates at synchronous speed in the inverse direction, i.e. anti-synchronous reference frame; the reason is explained shortly). Since zero-sequence currents cannot flow, only control of the components d , q , x' and y' is necessary, and it is done in the “current controllers” block (Fig. 4). The reference for the current d -component is again the only one that has a non-zero value, and it is obtained in the same manner as for the configuration of Fig. 3a. The current components x' and y' do not contribute to flux production, only to losses; thus they should be controlled to zero, the same as the q -component.

“Current controllers” block of Fig. 4 is presented separately in Fig. 7. It can be seen that the fundamental current control is performed with PI controllers in the same manner as in the previous subsection. Since there is no need for asymmetry or zero-sequence current control, the only remaining issue is then elimination of low-order harmonics. It is shown in [23] that the dominant harmonics in asymmetrical six-phase systems are -11^{th} and 13^{th} , which map into the first (α - β) plane, and the 5^{th} and -7^{th} , which map into the second (x' - y') plane. The first plane rotates in the synchronous direction, and -11^{th} and 13^{th} harmonics are seen in this reference frame as the -12^{th} and 12^{th} . Therefore they can be controlled with single VPI resonant controller placed in both the d - and q -axis (Fig. 7). In order to control harmonics from the second plane in a similar manner, the coordinate system of the second plane has to rotate in anti-synchronous direction (this is ensured in the rotational transformation matrix). In the x' - y' plane the 5^{th} and the -7^{th} harmonic are seen as the 6^{th} and -6^{th} , respectively, and they can be conveniently controlled with a single VPI controller placed in both axes (Fig. 7).

The output of current controllers is transformed (using now inverse rotational and inverse decoupling matrix for asymmetrical six-phase systems) and the voltage reference signals for the PWM block are obtained in this way. The modulation strategy is again carrier-based; however, it utilizes now the zero-sequence injection, so that better dc-bus voltage utilization can be achieved. Zero-sequence injection is applied to each set separately [24].

IV. EXPERIMENTAL RESULTS

Experiments are performed in order to validate the theory presented in Section II and the control algorithms described in Section III, as well as to provide experimental verification of the simulation results given in [15,16]. It has also to be noted again that, while the charging/V2G scheme of Fig. 1 is in

principle the same as in [15], the source of the two three-phase voltage systems with 180° phase shift is here a transformer with a single secondary that is kept in open-end winding configuration (instead of a transformer with two secondaries, as in [15]).

Experimental setup for both configurations is illustrated in Fig. 8, while the rig data are given in Appendix. Instead of a battery (and a dc-dc converter, if needed), an amplifier “Spitzenberger & Spies” is utilized in order to provide a constant isolated dc voltage. A resistor of 0.5Ω (not shown in Fig. 8) is placed between the amplifier and the voltage source converter in order to emulate battery’s internal resistance. Grid phase voltages are 240V rms, 50Hz. The switching frequency of the converter is 10kHz, and asymmetrical PWM [25] is used; thus the sampling frequency is 20kHz. The dead time is $6\mu\text{s}$. Control is performed in CC mode and the algorithm is implemented using dSPACE ds1006 processor board. The symmetrical configuration is considered first.

A. Symmetrical Six-Phase Configuration - Charging Mode

The reference value for the d -component of the transformer secondary current is set to $i_d^* = 2\text{A}$ (since power invariant three-phase decoupling transformation is utilized, corresponding machine’s phase current rms is 1.15A).

An advantage of this topology is that the dc-bus voltage does not have to be higher than the peak of the grid line-to-line voltage (assuming a transformer with 1:1 transformation ratio). Thus, the topology does not require high voltage semiconductors. This is a feature that is shared with the topology described in [13]. Indeed, the experiment is performed here with dc-bus voltage of 450V. It should be noted that the same advantage could be accomplished with the asymmetrical topology (Fig. 2) by decreasing voltage ratings of the two transformer secondaries.

In Fig. 9a grid voltage v_{ag} , grid current i_{ag} , and the battery charging current i_L are presented. It can be seen that the grid current is sinusoidal and in phase with the voltage, demonstrating near-unity power factor operation. The battery charging current is a dc component and has a value of $i_L = 1.65\text{A}$. Fig. 9b presents spectrum of the grid current i_{ag} . It can be seen that it contains zero-sequence harmonics (primarily the 3^{rd} , 9^{th} , and 15^{th}) since the experiment is performed with grounded neutral point N of the primary. These harmonics exist purely due to the non-ideal nature of the transformer. Additional measurements (not included here) show that they have the same absolute value in the transformer no-load test, when transformer secondary terminals are left open, as they have during charging or V2G operation with any reference.

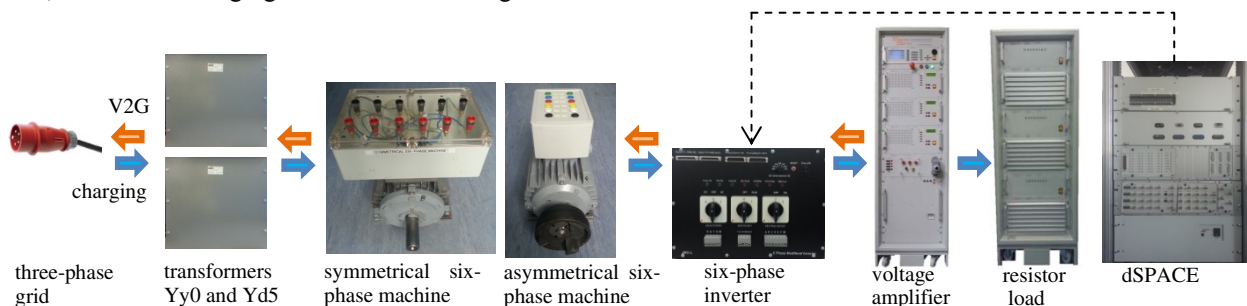


Fig. 8. Experimental rig.

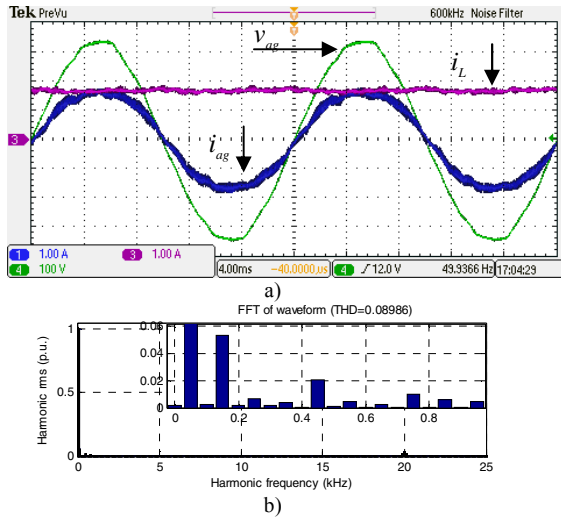


Fig. 9. a) Grid voltage v_{ag} , grid current i_{ag} , and battery charging current i_L , b) grid current spectrum.

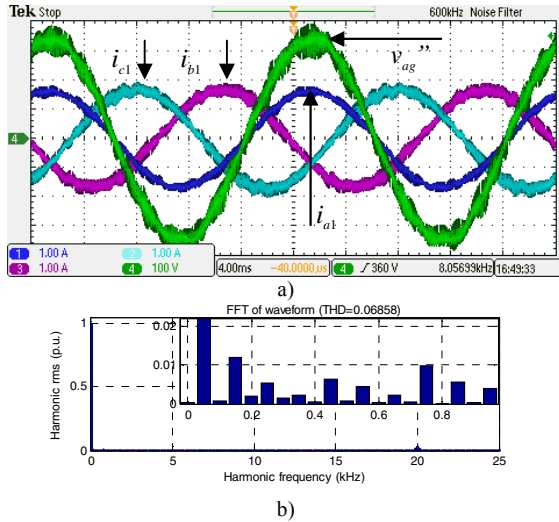


Fig. 10. a) Transformer secondary phase voltage v_{ag}'' and machine currents i_{a1} , i_{c1} and i_{b1} , b) machine current i_{a1} spectrum.

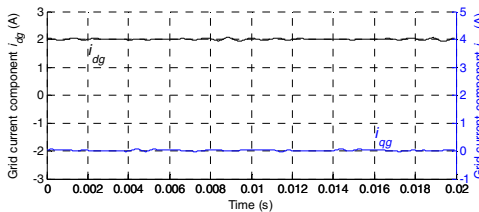


Fig. 11. Grid current components (on the transformer secondary side).

Thus, these harmonics are not a consequence of the dead time of the inverter. From Fig. 9b it can be seen that harmonics other than the zero-sequence ones are negligible (below 1% of the fundamental).

Fig. 10a shows machine currents i_{a1} , i_{c1} , and i_{b1} (which correspond to the secondary currents i_{ag} , i_{bg} and i_{cg} , respectively) in addition to the transformer voltage between two terminals of the phase “a” secondary winding v_{ag}'' (as noted, each of the three secondary phase windings has two accessible terminals, giving the total number of independent terminals as equal to six, Fig. 1). The unity power factor operation is obvious. By comparing the currents i_{a1} , i_{c1} and i_{b1} , it can be seen that i_{c1} and i_{b1} have higher ripple. This is due to

the unequal equivalent phase parameters of the machine during the charging/V2G mode, as explained in sub-section III-A (this should not be confused with the machine’s phase parameters in propulsion mode of operation, since the machine itself has identical phase parameters). Nonetheless, the fundamental rms values of these two currents are the same and this validates the control part of Fig. 6 that deals with the asymmetry control. Machine current i_{a1} spectrum is given in Fig. 10b and it indicates excellent current quality with negligible low order harmonics (below 1% of the fundamental). Since the transformer secondary does not contain a neutral point, harmonics that are multiples of three now can flow, regardless of whether the transformer primary neutral point N is grounded or not. Indeed, machine i_{a1} current spectrum in Fig. 10b shows that it does contain the 3rd and 9th harmonics. However, the triplen harmonics are controlled well by zero-sequence current control of Fig. 6 and are of acceptably low values. It should be noted that, with respect to Fig. 6, the zero-sequence current control in the experiment, in addition to the control of the 3rd harmonic, controls also the 9th harmonic, in the similar manner as shown in Fig. 6 for the 3rd harmonic. Namely, another block similar to the one shown at the bottom of Fig. 6 is added in parallel to the existing one. The only difference is in the parameter “harmonic number”, which now has a value of 9, rather than 3.

Transformer secondary side current components after rotational transformation are shown in Fig. 11. The q -component is controlled at zero, and d -current component follows its reference without a steady-state error. Fig. 11 also confirms unity power factor operation as well as balanced operation, since traces do not contain the second harmonic.

Machine current components, obtained by transforming oscilloscope current recordings, are depicted in Fig. 12. As predicted by (4)-(5) the charging process utilizes only α - and γ -component. Since the β -component is controlled at zero, only a pulsating field exists in the machine, which is, however, not capable of producing a starting torque. Thus the machine stays at standstill. Fig. 12 further shows that the β -component is not only zero on average, but it is also instantaneously equal to zero, i.e. it does not contain any high-frequency ripple. As a consequence, there is not any torque ripple being generated during the charging process.

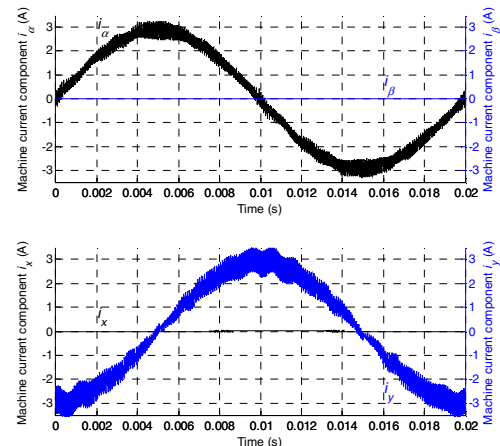


Fig. 12. Machine current components (from oscilloscope recordings).

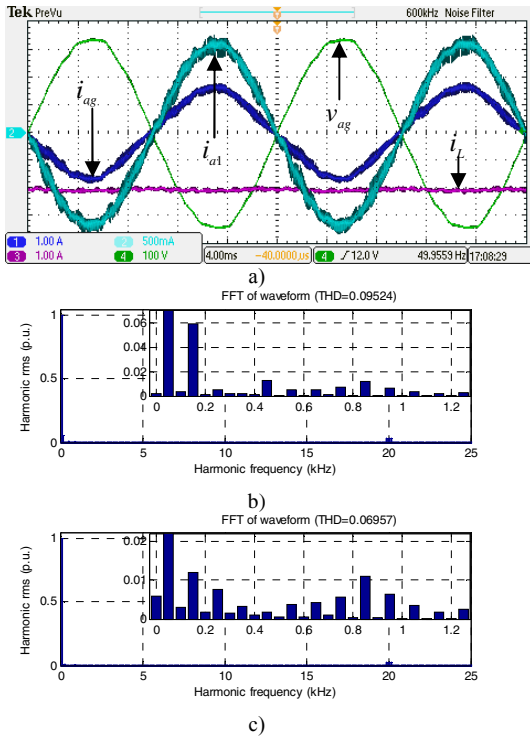


Fig. 13. a) Grid phase voltage v_{ag} , grid current i_{ag} , machine current i_{a1} and battery charging current i_L , b) grid current spectrum, c) machine current spectrum.

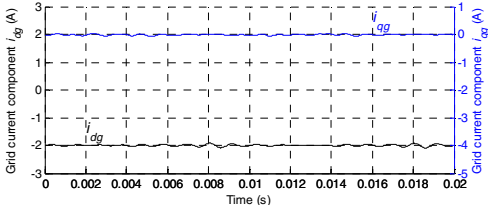


Fig. 14. Grid current components (on the transformer secondary side).

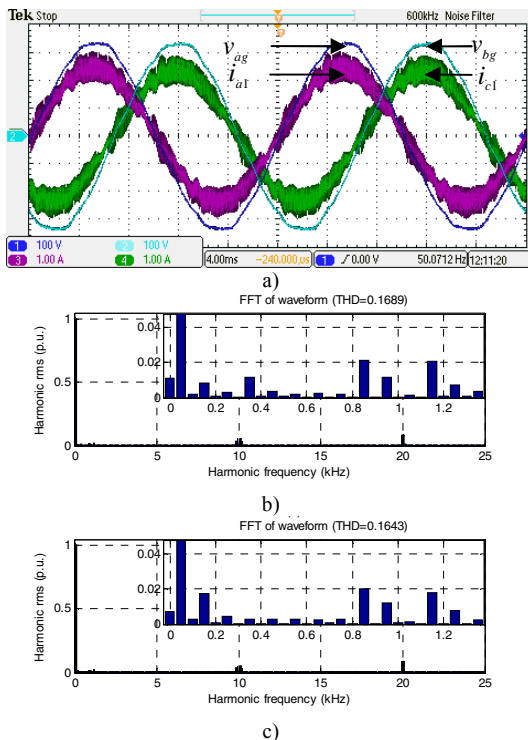


Fig. 15. a) Grid phase voltages v_{ag} , v_{bg} and machine currents i_{a1} , i_{c1} , b) spectrum of machine current i_{a1} c) grid current i_{ag} spectrum.

B. Symmetrical Six-Phase Configuration - V2G Mode

By changing the reference current from $i_d^* = 2A$ to $-2A$ the configuration automatically enters V2G mode (the control is unaltered and is in the CC mode). From Fig. 13a it can be seen that the grid current i_{ag} is in phase opposition with the grid phase voltage v_{ag} , which yields a unity power factor in V2G mode. Battery charging current is again a dc component with a value of $i_L = -2.05A$, and it contains very little ripple. Compared to Fig. 9a this current is higher by absolute value since in V2G mode battery power has to be higher than the grid-side power to cover the losses, while in the charging mode the battery charging power is lower than the grid-side power due to the losses being covered from the grid. Fig. 13b and Fig. 13c demonstrate very good current quality in this mode as well (low order harmonics of the machine current i_{a1} are again below 1% of the fundamental, and the same considerations as in charging mode apply to the 3rd harmonic of the grid current, which is not introduced by the inverter).

Grid current components are presented in Fig. 14, and while the q -component is again kept at zero, the d -component follows its reference without a steady-state error. Fig. 14 confirms unity power factor operation and balanced control in the V2G mode of operation.

C. Asymmetrical Six-Phase Configuration - Charging Mode

In this and the next subsection experimental results in charging and V2G mode are given for the configuration of Fig. 2. Instead of a single transformer with two secondary windings, two transformers with connections Yy0 and Yd5 are employed. The transformers have their primary sides connected to the same three-phase grid and have such transformation ratios that on the output they give asymmetrical six-phase voltage supply of the same phase voltage value, namely 240V rms. Transformer neutral points are not grounded.

The dc-bus voltage is set to 720V. It is increased compared to the symmetrical topology. The reason for this is that it has to be higher than the grid line-to-line voltage, while in the case of the symmetrical topology it had to be higher than peak of the grid phase voltage. The configuration is controlled in the constant current (CC) mode by the algorithm shown in Fig. 7. The grid current reference i_d^* is set to 4A for the charging process. In Fig. 15a grid phase voltages v_{ag} , v_{bg} and machine currents i_{a1} , i_{c1} are presented. The balanced operation with unity power factor is evident. Both phase currents now have the same ripple since there is no field in the machine to introduce asymmetry in the equivalent charging/V2G scheme. The relatively high current ripple is due to the small machine leakage inductance in the x - y plane (which is, according to (9)-(10), the plane through which the power is transferred) which is, due to the stator winding design of the used machine, more than ten times lower than in the first plane. Machine current i_{a1} spectrum is given in Fig. 15b, and it contains only small low order harmonics. The grid current i_{ag} is of almost identical shape, as is evidenced with the spectrum in Fig. 15c, although its amplitude is two times higher (since three grid currents are transformed into six currents at the output of the transformer).

Grid current components are given in Fig. 16. While q -, x - and y -component are kept at zero, the d -component has a non-

zero value and it follows the reference well. The small ripple that can be seen in Fig. 16 is a consequence of the mapping of current low-order harmonics, whose presence is evident from Figs. 15b and 15c. On the other hand, if machine current components are observed (Fig. 17), it can be seen that the charging process utilizes only the second plane, leaving the field/torque-producing plane without excitation. Since the field is not produced in the machine, there is no torque production and, consequently, no rotor movement.

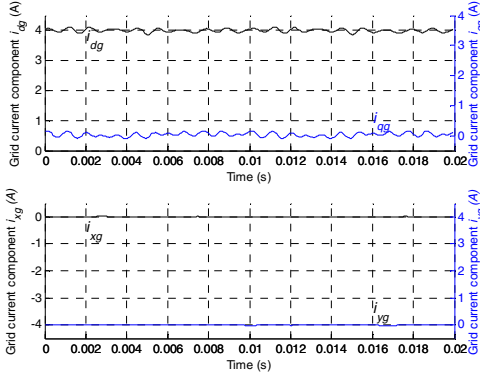


Fig. 16. Grid current components (on the transformer secondary side).

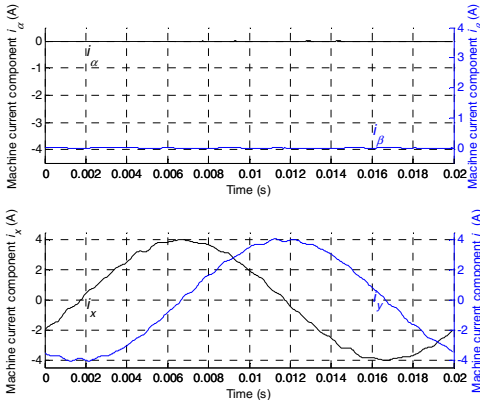


Fig. 17. Machine current components.

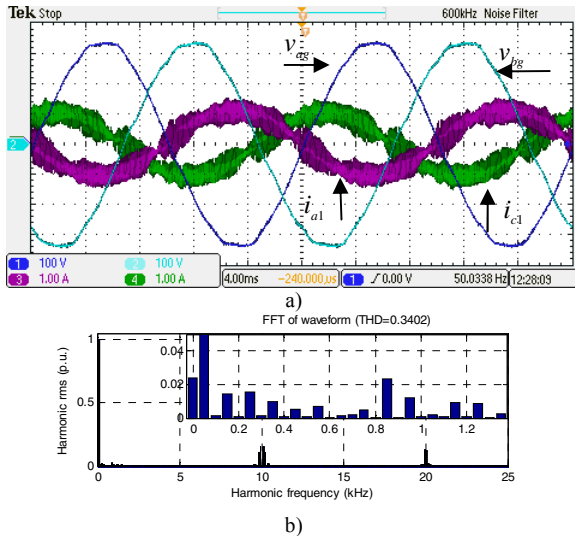


Fig. 18. a) Grid phase voltages v_{ag} , v_{bg} and machine currents i_{a1} , i_{c1} . b) spectrum of machine current i_{a1} .

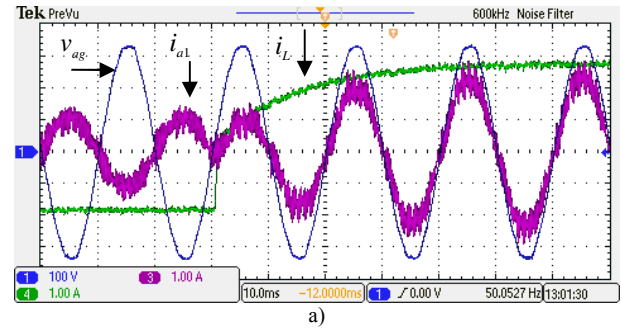


Fig. 19. Transient from V2G ($i_d^* = -2A$) into the charging mode ($i_d^* = 4A$): a) grid voltage v_{ag} , machine phase current i_{a1} and battery charging current i_L , b) grid current components i_{dg} and i_{qg} .

D. Asymmetrical Six-Phase Configuration – V2G Mode

V2G mode is performed with the reference $i_d^* = -2A$. Fig. 18a shows that the currents i_{a1} , i_{c1} are shifted by 180° with respect to the voltages, representing again unity power factor operation. It can be seen that the currents are balanced. Machine current i_{a1} spectrum (Fig. 18b) again contains only small low order harmonics.

Finally, a transient from V2G into the charging mode is initiated by changing the reference in a step-wise manner to $i_d^* = 4A$. Grid phase voltage v_{ag} , machine current i_{a1} , and battery charging current are depicted in Fig. 19a, which clearly shows fast transient response. Battery charging current i_L is negative in V2G mode and has a value of $-1.9A$. During the transient it gradually increases to reach the final value of $i_L = 2.9A$ in the charging mode. Grid current components during the transient are shown in Fig. 19b. The q -component does not deviate from zero during the transient, while the d -component quickly reaches its new reference.

It should be noted here that resolver readings were continuously monitored in both symmetrical and asymmetrical configuration and in all operating modes, and that they proved that the rotor does not move (even in transients). Since each time the traces were completely uniform (and of zero value, similar to [12]) authors chose to omit them from the paper.

Last but not least, a remark related to the grid current harmonic content is due. It is evident from the presented results that, in both charging and V2G modes, the grid current does not contain low-order harmonics but it inevitably contains high-frequency switching harmonics. This will always be the case if a PWM rectifier is used. As long as the switching frequency is more than 40 times the grid frequency (over 2kHz in the 50Hz grid), these harmonics will be outside the current standards and hence can be freely injected in the grid. However, the situation may well change in future when EVs with fast charging capability become more wide-spread. Some of the current standards for electric vehicles can be found in [26].

V. CONCLUSION

The paper analyses two integrated and isolated charging configurations, incorporating a symmetrical and an asymmetrical six-phase machine, respectively, into the charging process. Isolation takes place outside the vehicle, in the charging station. Phase transposition principle is employed in order to avoid torque production in the machines. The paper also introduces a symmetrical six-phase supply topology based on the open-end winding transformer secondary and develops in detail enhanced control schemes for both configurations. Experimental results are used to validate the unity power factor, torque-free operation for both symmetrical and asymmetrical configurations, in both charging and V2G mode.

The main advantageous features of the developed solutions are the following characteristics: i) the propulsion motor and the propulsion converter are fully integrated in the charging/V2G process, ii) charging/V2G operation takes place without electromagnetic torque production, so that mechanical braking is not required, iii) post-fault operation in propulsion, required for the 'limp-home' mode, is rather simple to realise by software reconfiguration, iv) galvanic isolation is obtained using transformers which are situated off-board, and v) single-phase (slow) charging is readily achievable.

A drawback, believed to be minor and significantly outweighed with the listed advantages, is that there is a need for hardware reconfiguration, using four added switches. However, it should be noted that both topologies require a line-frequency transformer, which can be bulky, and hence this should be carefully weighed against the main benefit, isolation between the vehicle and the grid.

As a final remark, the issue of which of the two topologies is better for the real world applications needs to be addressed. There appears to be no clear winner. As far as the propulsion mode is concerned, the preference is always given to the asymmetrical six-phase machine [18]. However, from the point of view of charging/V2G mode, symmetrical version is more favourable since the off-board transformer is just a three-phase one, with the secondary in OeW configuration.

APPENDIX: EXPERIMENTAL EQUIPMENT DATA

Symmetrical six-phase induction machine: the parameters are $R_s = 3.6\Omega$, $R_r = 1.8\Omega$, $L_m = 205\text{mH}$, $L_{ys} = 8.1\text{mH}$, $L_{yr} = 11.5\text{mH}$. Other data: three pole pairs, 50 Hz, 110 V (phase-to-neutral), 1.1kW, 900 rpm.

Asymmetrical six-phase induction machine: the parameters are $R_s = 12.5\Omega$, $R_r = 6\Omega$, $L_m = 590\text{mH}$, $L_{ys} = 61.5\text{mH}$, $L_{yr} = 11\text{mH}$. Six-pole, obtained by rewinding a 380 V, 50 Hz, 1.1 kW three-phase machine.

Dc source/sink: "Spitzenberger & Spies" – two DM 2500/PAS systems connected in series. Power sinking up to 4kW is enabled by an additional resistive load RL 4000, which is shown in Fig. 8 and is labelled as 'resistor load'.

Controller: dSPACE DS1006 processor board. DS2004 high-speed A/D board and DS5101 Digital Waveform Output Board are used for the A/D conversion of measured signals and PWM signal generation. Incremental Encoder Interface Board DS3002 is used to validate that machines do not move during the charging/V2G process.

Converter: Custom made eight-phase inverter with EUPEC

FS50R12KE3 IGBTs. Using the heat-sink data, it is estimated that the rated continuous output rms current is 14A, which gives for a 240V rms phase voltage for six phases of inverter continuous rating of approximately 20kVA.

REFERENCES

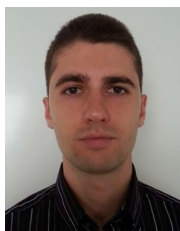
- [1] A. Khaligh, S. Dusmez, "Comprehensive topological analysis of conductive and inductive charging solutions for plug-in electric vehicles," *IEEE Trans. Vehicular Techn.*, vol. 61, no. 8, pp. 3475-3489, 2012.
- [2] S. Haghbin, S. Lundmark, M. Alakula, and O. Carlson, "Grid-connected integrated battery chargers in vehicle applications: review and new solution," *IEEE Trans. Ind. Electron.*, vol. 60, no. 2, pp. 459-473, 2013.
- [3] L. De Sousa, B. Silvestre, and B. Bouchez, "A combined multiphase electric drive and fast battery charger for electric vehicles," in *Proc. IEEE Vehicle Power and Propulsion Conference VPPC*, Lille, France, 2010.
- [4] S. Liu, S. Hahlbeck, T. Schoenen, K. Hameyer, "An integrated on-board charger with direct grid connection for battery electrical vehicle," in *Proc. Int. Symposium on Power Electronics, Electric Drives, Automation and Motion SPEEDAM*, Sorrento, Italy, pp. 335-340, 2012.
- [5] D. Thimmesch, "An SCR inverter with an integral battery charger for electric vehicles," *IEEE Trans. Ind. Appl.*, vol. IA-21, no. 4, pp. 1023-1029, 1985.
- [6] A. G. Cocconi and W. E. Rippel, "Integrated motor drive and recharge system," *US Patent* No. US 5,099,186 A, 1992.
- [7] A. G. Cocconi, "Combined motor drive and battery recharge system," *US Patent*, No. US 5,341,075 A, 1994.
- [8] S. Seung-Ki and L. Sang-Joon, "An integral battery charger for four-wheel drive electric vehicle," *IEEE Trans. Ind. Appl.*, vol. 31, no. 5, pp. 1096-1099, 1995.
- [9] L. Solero, "Nonconventional on-board charger for electric vehicle propulsion batteries," *IEEE Trans. Vehicular Techn.*, vol. 50, no. 1, pp. 144-149, 2001.
- [10] L. Jianing, X. Guoqing, J. Linni, and L. Liu, "Electric air conditioner system with on-board charger for PHEV," in *Proc. IEEE Int. Conf. on Information and Automation ICIA*, Shenzhen, China, pp. 421-426, 2011.
- [11] C. Hung-Chun and L. Chang-Ming, "An integrated driving/charging switched reluctance motor drive using three-phase power module," *IEEE Trans. Ind. Electron.*, vol. 58, no. 5, pp. 1763-1775, 2011.
- [12] I. Subotic, N. Bodo, E. Levi, M. Jones, "On-board integrated battery charger for EVs using an asymmetrical nine-phase machine," *IEEE Trans. Ind. Electron.*, accepted for publication, DOI: 10.1109/TIE.2014.2345341.
- [13] S. Loudot, B. Briane, O. Ploix, and A. Villeneuve, "Fast charging device for an electric vehicle," *US Patent*, No. US 2012/0286740 A1, 2013.
- [14] S. Haghbin, I. S. Guillen, "Integrated motor drive and non-isolated battery charger based on the torque cancelation in the motor," in *Proc. IEEE Int. Conf. on Power Electronics and Drive Systems PEDS*, Kitakyushu, Japan, pp. 824-829, 2013.
- [15] I. Subotic, E. Levi, "An integrated battery charger for EVs based on a symmetrical six-phase machine," in *Proc. IEEE Int. Symp. on Ind. Electronics ISIE*, Istanbul, Turkey, pp. 2070-2075, 2014.
- [16] I. Subotic, E. Levi, M. Jones, and D. Graovac, "An integrated battery charger for EVs based on an asymmetrical six-phase machine," in *Proc. IEEE Industrial Electronics Society Conf. IECON*, Vienna, Austria, pp. 7242-7247, 2013.
- [17] E. Levi, M. Jones, S.N. Vukosavic, and H.A. Toliyat, "A novel concept of a multiphase, multimotor vector controlled drive system supplied from a single voltage source inverter," *IEEE Trans. Power Electron.*, vol. 19, no. 2, pp. 320-335, 2004.
- [18] E. Levi, R. Bojoi, F. Profumo, H.A. Toliyat, and S. Williamson, "Multiphase induction motor drives - a technology status review," *IET Electr. Power Appl.*, vol. 1, no. 4, pp. 489-516, 2007.
- [19] L. R. Limongi, R. Bojoi, C. Pica, F. Profumo and A. Tenconi, "Analysis and comparison of phase locked loop techniques for grid utility applications," in *Proc. Power Conversion Conf. PCC*, Nagoya, Japan, pp. 674-681, 2007.
- [20] S. Dusmez, A. Cook, and A. Khaligh, "Comprehensive analysis of high quality power converters for level 3 off-board chargers," in *Proc. IEEE Vehicle Power and Propulsion Conf. VPPC*, Chicago, Illinois, CD-ROM, 2011.
- [21] C. Lascu, L. Asiminoaei, I. Boldea, and F. Blaabjerg, "High

performance current controller for selective harmonic compensation in active power filters,” *IEEE Trans. Power Electron.*, vol. 22, no. 5, pp. 1826-1835, 2007.

- [22] A. G. Yepes, “Digital resonant current controllers for voltage source converters,” *PhD Thesis*, University of Vigo, Vigo, Spain, 2011.
- [23] H. S. Che, E. Levi, M. Jones, W. P. Hew, and N. A. Rahim, “Current control methods for an asymmetrical six-phase induction motor drive,” *IEEE Trans. Power Electron.*, vol. 29, no. 1, pp. 407-417, 2014.
- [24] D. Dujic, E. Levi, and M. Jones, “Dc bus utilization in multiphase VSI supplied drives with a composite stator phase number,” in *Proc. IEEE Int. Conf. on Industrial Technology ICIT*, Viña del Mar, Chile, pp 1495-1500, 2010.
- [25] D. G. Holmes and T. A. Lipo, “Pulse width modulation for power converters: principles and practice,” *IEEE Press*, Piscataway, NJ, 2003.
- [26] M. Yilmaz and P. T. Krein, “Review of battery charger topologies, charging power levels, and infrastructure for plug-in electric and hybrid vehicles,” *IEEE Trans. Power Electron.*, vol. 28, no. 5, pp. 2151-2169, 2013.



Victor Levi (S'89, M'91, SM'13) received his MSc and PhD degrees from the University of Belgrade, Yugoslavia, in 1986 and 1991, respectively, both in Electrical Engineering. From 1982 until 2001 he was with the University of Novi Sad, Yugoslavia, where he became full Professor in 2001. He worked at the University of Manchester from 2001 until 2003, and then in the United Utilities and Electricity North West from 2003 until 2013. In 2013 he rejoined the University of Manchester as a Senior Lecturer.



Ivan Subotic (S'12) received the Dipl. Ing. and MSc degrees in Electrical Engineering from the University of Belgrade, Belgrade, Serbia, in 2010 and 2011, respectively. Since 2011, he has been with the Liverpool John Moores University, Liverpool, U.K., as a PhD student. His main research interests include power electronics, electric vehicles, and control of multiphase drive systems.



Nandor Bodo received his Masters degree in 2009 in Power Electronics from the University of Novi Sad, Faculty of Technical Sciences, Novi Sad, Serbia and his PhD degree in Electrical Engineering in 2013 from Liverpool John Moores University, Liverpool, UK. He is currently with the Liverpool John Moores University, Liverpool, UK as a post-doctoral research associate. His research interests include power electronics and variable speed drives.



Emil Levi (S'89, M'92, SM'99, F'09) received his MSc and the PhD degrees in Electrical Engineering from the University of Belgrade, Yugoslavia in 1986 and 1990, respectively. From 1982 till 1992 he was with the Dept. of Elec. Engineering, University of Novi Sad. He joined Liverpool John Moores University, UK in May 1992 and is since September 2000 Professor of Electric Machines and Drives. He served as a Co-Editor-in-Chief of the *IEEE Trans. on Industrial Electronics* in the 2009-2013 period and is currently Editor-in-Chief of the *IET Electric Power Applications* and an Editor of the *IEEE Trans. on Energy Conversion*. He is the recipient of the Cyril Veinott award of the IEEE Power and Energy Society for 2009 and the Best Paper award of the *IEEE Trans. on Industrial Electronics* for 2008. In 2014 he received the “Outstanding Achievement Award” from the European Power Electronics (EPE) Association.



Martin Jones received his BEng degree (First Class Honours) in Electrical Engineering from the Liverpool John Moores University, UK in 2001. He was a research student at the Liverpool John Moores University from September 2001 till Spring 2005, when he received his PhD degree in Electrical Engineering. Dr Jones was a recipient of the IEE Robinson Research Scholarship for his PhD studies and is currently with Liverpool John Moores University as a Reader. His research is in the area of high performance ac drives.